Construction of Optimal SERS Hotspots Based on Capturing the Spike Receptor-Binding Domain (RBD) of SARS-CoV-2 for Highly Sensitive and Specific Detection by a Fish Model

Guangyao Huang, Hongxin Zhao, Pan Li,* Juanjuan Liu, Siyu Chen, Meihong Ge, Miao Qin, Guoliang Zhou, Yongtao Wang, Shaofei Li, Yizhuang Cheng, Qiang Huang, Junfeng Wang, Hongzhi Wang,* and Liangbao Yang*

Cite This: https://doi.org/10.1021/acs.analchem.1c03807

Read Online

ACCESS | Metrics & More | Article Recommendations | Supporting Information

ABSTRACT: It is highly challenging to construct the best SERS hotspots for the detection of proteins by surface-enhanced Raman spectroscopy (SERS). Using its own characteristics to construct hotspots can achieve the effect of sensitivity and specificity. In this study, we built a fishing mode device to detect the receptor-binding domain (RBD) of severe acute respiratory syndrome coronavirus 2 (SARS-CoV-2) at low concentrations in different detection environments and obtained a sensitive SERS signal response. Based on the spatial resolution of proteins and their protein-specific recognition functions, SERS hotspots were constructed using aptamers and small molecules that can specifically bind to RBD and cooperate with Au nanoparticles (NPs) to detect RBD in the environment using SERS signals of beacon molecules. Therefore, two kinds of AuNPs modified with aptamers and small molecules were used in the fishing mode device, which can specifically recognize and bind RBD to form a stable hotspot to achieve high sensitivity and specificity for RBD detection. The fishing mode device can detect the presence of RBD at concentrations as low as 0.625 ng/mL and can produce a good SERS signal response within 15 min. Meanwhile, we can detect an RBD of 0.625 ng/mL in the mixed solution with various proteins, and the concentration of RBD in the complex environment of urine and blood can be as low as 1.25 ng/mL. This provides a research basis for SERS in practical applications for protein detection work.
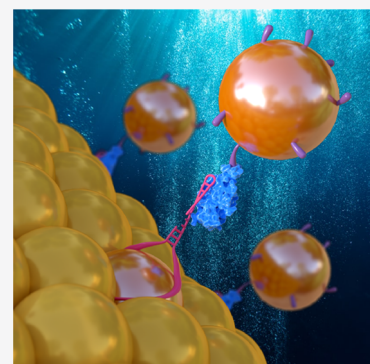
INTRODUCTION

Surface-enhanced Raman spectroscopy (SERS) is an effective and nondestructive analytical technique for detecting bio-molecules.[1,2] However, despite the theoretical excellence in terms of molecular recognition, the considerably weak intensity of Raman scattering has been a major drawback in its application.[3] There are high-field intensity region hotspots (the gap between nanoparticles is less than 10 nm), which are generated in the metal plane of nanoparticles (NPs) and support plasmon resonance.[1,4] When SERS provides solutions to some major problems, the enhancement of low concentrations, an increase in the number of "hotspots", and high stability are often expected.[5,6] The construction of "immobilization" hotspots on solid substrates by fabricating directional assemblies of functional nanoparticles is a frontier research field in the field of SERS. However, electromagnetic enhancement is highly distance-dependent.[7] To maximize the hotspots experienced by a molecule, one of the most critical issues has been subnanometer control of the gap size.[8] Furthermore, in complex environments, there are also great challenges regarding how the target to be measured enters the hotspot area. Therefore, researchers continue to explore hotspots at the same time, and the application of biological sample detection is also gradually being explored in depth. SERS exhibits great potential in clinical diagnosis due to low susceptibility to environmental variables and the miniature/portable instruments used for in situ detection, and it uses nondestructive methods to offer highly sensitive, timely, and accurate information.[9,10] Several different detection methods have been developed recently to meet the urgent need for rapid and sensitive detection of clinically relevant viruses.[11-13] Of these, the SERS detection method is considered a strong candidate because of its ultrasensitive detection capability.[14-16]

With SERS, proteins can be detected both directly and indirectly.[5,17] Direct detection involves analysis of the intrinsic Raman spectrum of the protein of interest in a simple, label-free manner, which is very attractive because it is very sensitive at the single-molecule level.[18,19] However, only a few target proteins with high binding affinity to the NPs surface and

strong signal intensity can be analyzed by direct detection. In contrast, indirect detection using SERS probes can offer rapid analysis because degenerate detection typically employs nanoproteins functionalized with Raman dyes as tags and antibodies (SERS probes).[20,21] However, the spatial resolution of protein−antibody binding affects the localized surface plasmon resonance (LSPR) between SERS substrates, thereby reducing the SERS signal for protein detection. Unfortunately, the low SERS cross section of polymers (including biopolymers) is well known[2] and results in the limited availability of applicable peptides or proteins. Therefore, this method cannot solve the problem of random and uneven hotspots, which affects signal stability in SERS detection. To improve the sensitivity, selectivity, and stability of SERS-based detection, researchers have sought new solutions that replace antibodies in detection. Due to the chemical properties of nucleic acids, aptamers can be chemically synthesized and precisely modified, and they exhibit high thermal stability, little batch-to-batch variation, and specific binding to target proteins.[22] Because of the small size of aptamers (approximately 2−3 nm in diameter) compared with antibodies (approximately 12−15 nm in diameter), aptamers are more suitable for the development of a method for SERS detection of proteins.[22] Studies have shown that SERS specifically binds proteins by aptamers to enhance the sensitivity of SERS to detect proteins.[23−25] Therefore, two kinds of aptamers can be used to replace antibodies to modify the specific binding with proteins on NPs and mediate the construction of hotspots within 10 nm. Unfortunately, the binding domains of different aptamers and proteins will have crossed parts, the existence of spatial conformations between aptamers and proteins is difficult to control, and there are still gaps between NPs that are greater than 10 nm. At this time, replacing one of the aptamers with a small molecule that specifically binds to the protein would largely solve this problem. Moreover, the spatial resolution of small-molecule compounds is very small, which effectively closes the distance between NPs and forms hotspots.

Severe acute respiratory syndrome coronavirus 2 (SARS-CoV-2)—a member of the subgenus Sarbecovirus—has spread globally.[26−28] According to previous reports, the S protein is critical for adhering to host cells, and the receptor-binding domain (RBD) of the S protein mediates the interaction with angiotensin-converting enzyme 2 (ACE2).[29] When viruses enter host cells, spike glycoproteins bind to specific cell surface receptors through their RBD to facilitate viral invasion into host cells.[30] This makes the RBD of the SARS-CoV-2 spinous glycoprotein a key target for the diagnosis, treatment, and vaccination of SARS-CoV-2.[31] Therefore, the detection of RBD can reflect the existence of SARS-CoV-2 virus.

In this study, we developed a fishing mode SERS detection device (fishing mode device) based on RBD protein characteristics. Given the complex environment for virus detection, we adopted a portable and easy-to-sample platform—Ag acupuncture needle (AgAN).[32,33] According to the size (4−6 nm) and characteristics of the RBD, aptamers and small molecules can be selected to connect with the RBD. After the aptamers and small molecules are modified on the AuNPs, the RBD is connected like a fishhook, and stable hotspots of 6−9 nm in size are formed between the two AuNPs, which ensures the specificity, sensitivity, and stability of detection. Therefore, using the characteristics of biological proteins, we developed a new SERS detection mode with high specificity, high sensitivity, and high stability.

■ EXPERIMENTAL SECTION

Reagents. Malachite, poly(vinylpyrrolidone) PVP (MW = 55 000), NH$_2$OH HCl, crystal violet (CV), sodium citrate, and hydrogen tetrachloroaurate (HAuCl$_4$·4H$_2$O) were purchased from Shanghai Chemicals Company. 2-Acetamido-2-deoxy-β-D-glucopyranose (NAG) (A118965) was purchased from Aladdin (Shanghai, China), and 4-mercaptophenylboronic acid (MPBA) (M814076) was purchased from Macklin (Shanghai, China). A Millipore water purification system was used to produce ultrapure water (18.2 MΩ cm). Oligonucleotides were purchased from Sangon Biotech (Shanghai, China). The aptamer variants were modified with an amido group at the 5′ end. The aptamer sequence we used was that of the aptamer previously reported for this target:[22] 5′-NH$_2$-CAGCACCGACCTTGTGCTTTGGGAGTGCTGGTC-CAAGGGCGTTAATGGACA-3′. AgAN was purchased from Suzhou Tianxie Acupuncture Instrument Co., Ltd. RBD was synthesized, purified, and separated in the laboratory of Prof. Junfeng Wang, High Magnetic Field Science Center, Hefei Institutes of Physical Science, Chinese Academy of Sciences.

Apparatus. Scanning electron microscopy (SEM) images were taken with an Auriga focused ion-beam scanning electron microscopy (FIB-SEM) system. Ultraviolet−visible (UV−vis) absorption spectra (UV-2550, Shimadzu, Japan) were used to determine the optical properties of Cit-AuNPs and PVP-AuNPs. Fourier transform infrared (FTIR) spectra were obtained with a Nicolet 8700 spectrometer (America). Liquid chromatography−mass spectrometry (LC−MS) data was obtained with an Agilent 1290/6540 (America) LC−MS system. SERS spectra were collected by a Raman spectrometer (SEED 3000, Ocean hood, China) with a 785 nm laser. The laser focal spot on the metal surface was approximately 100 μm in diameter with a measured power of 200 mW and recorded with a 1 s accumulation time.

Preparation of RBD Protein. A gene encoding SARS-CoV-2 receptor-binding domain (RBD, residues Arg319−Phe541) was synthesized by General Biosystems (Anhui) Co., Ltd. The RBD gene was amplified and connected with the C-terminal tobacco etch virus (TEV)-Fc tagged encoding gene by polymerase chain reaction (PCR). Then, the RBD-TEV-hFc DNA fragments were subcloned into the protein expression vector and transformed into the *Escherichia coli* strain DH5α and plasmids were harvested. The RBD-TEV-hFc recombinant proteins were expressed in Expi293F cells at a density of 3 × 10^6 cells/mL. the supernatants were collected after 48 h. Then, the supernatant containing RBD-TEV-hFc was affinity-purified by protein A FF (GE Healthcare). The bound protein was eluted with 0.1 M glycine−HCl (pH 3.0) and collected into tubes containing 1 M Tris−HCl (pH 9.0) to neutralize the pH. The fusion proteins were finally dialyzed against 20 mM phosphate-buffered saline (PBS) (pH 7.2). The Fc fragments were removed using Protein A chromatography after incubation with TEV protease at 30 °C for 1 h. The RBD protein was further purified by gel filtration (Superdex-75, GE Healthcare) TH chromatography using an AKTA FPLC system. The purified RBD was identified by LC−MS/MS spectrometry and analyzed by Proteome Discoverer software (Thermo Fisher Scientific).

Preparation of PVP-Stabilized AuNPs (PVP-AuNPs). A seed particle solution was synthesized by reducing HAuCl$_4$
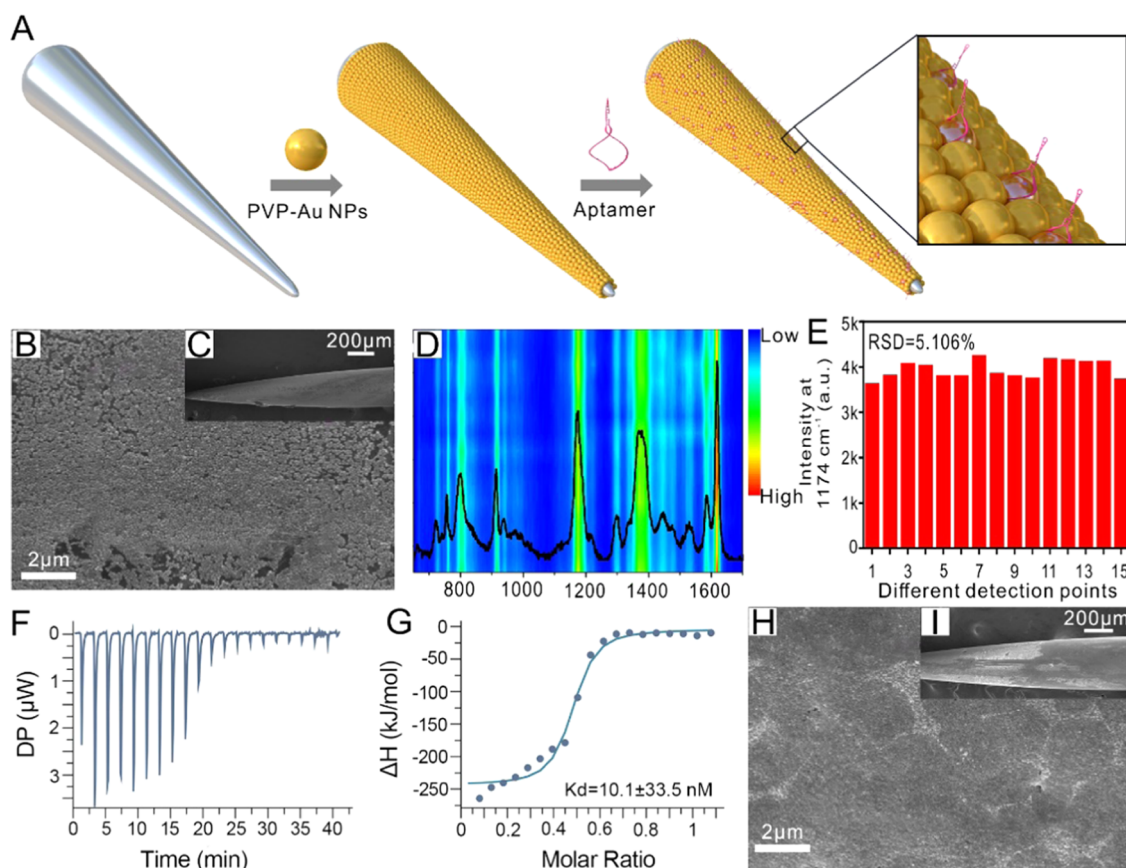
Figure 1. Preparation of AgAN-Au-Apt and characterization of material properties. (A) Schematic of the fabrication process of AgAN-Au-Apt. (B, C) SEM was used to characterize the photos of AuNPs on the AgAN. (D) Using AgAN modified with AuNPs, 15 SERS signals were detected for CV in different regions, and a heat map was made. SERS spectra were performed on a Lab-RAM HR800 spectrometer with a 633 nm laser excitation source and recorded with 1 s accumulation time. The laser focal spot on the metal surface was about 0.9 μm in diameter with a measured power of 0.89 mW. (E) According to the result of (D), the signal intensity of 1174 cm^{-1} peak position of AuNPs on AgAN for CV detection was calculated, and the relative standard deviation (RSD) of 15 SERS signals was calculated. (F, G) Results of the interaction between the aptamer and RBD were detected by ITC. (H, I) SEM characterization of the aptamer-modified AuNPs on AgAN.

with citrate.[33] In the first step, 1 mL of 1% HAuCl$_4$ solution was added to a 250 mL three-necked flask containing 99 mL of ultrapure water and then heated to boiling with magnetic stirring. At the beginning of boiling, 5 mL of 1% trisodium citrate solution was injected rapidly and boiling was continued for 30 min. The color of the solution was wine red at the end. In the second step, PVP-stabilized AuNPs were prepared in water. Twenty-five milliliters of seed solution was added to a three-necked, round-bottom flask. Then, the seed solution was stirred violently at room temperature. One milliliter of 1% PVP aqueous solution, 20 mL of 0.02% NH$_2$OH·HCl solution, and 1 mL of 1% sodium citrate solution were injected into the seed solution. When 20 mL of 0.1% (w/v) HAuCl$_4$ was added to the solution at a rate of 1 mL/min, the resulting particles (55 nm, 5.68×10^{12} NPs/mL) were coated with PVP and thus well suspended in water.

Preparation of AgAN-Au NP-Aptamer (AgAN-Au-Apt). Ag acupuncture needles (AgANs) with a diameter of 0.40 mm were washed three times with ethanol and acetone. AgANs were then dried using nitrogen and heated at 60 °C for 30 min. After drying, the AgANs were immersed in a concentrated solution of PVP-AuNPs for 12 h and then heated at 60 °C for 30 min. Then, AgAN-Au-Apt was prepared by immersing the needle in the solution containing the aptamer (10 μM) for 4 h.

Preparation of NAG-MPBA-AuNPs (N-M-Au). Reversible covalent bonds between MPBA and 1,2-/1,3-cis-diols in aqueous solution are widely used for the construction of molecular receptors.[34−36] In aqueous solution, NAG and MPBA were mixed in a 1:1 ratio and reacted for 24 h in the dark at room temperature. NAG-MPBA (the linker between NAG and MPBA) with a concentration of 1×10^{-5} M was mixed with PVP-AuNPs and reacted for 4 h in the dark at room temperature. N-M-Au was obtained.

Formation of Fishing Mode Device (AgAN-Au-Apt-RBD-N-M-Au). The as-prepared AgAN-Au-Apt was placed in a liquid environment containing RBD and incubated at 37 °C for 10 min. At this time, AgAN-Au-Apt-RBD was formed. Then, the AgAN-Au-Apt was removed and cleaned three times using PBS to remove nonspecific adsorption on the surface of AgAN-Au-Apt-RBD. Furthermore, AgAN-Au-Apt-RBD was put into N-M-Au solution, incubated at 37 °C for 10 min to form AgAN-Au-Apt-RBD-N-M-Au, and then washed three times after retrieval using PBS. Afterward, SERS analysis (power = 100 mW, integration time = 2 s) was performed with a portable Raman spectrometer (SEED 3000, Oceanhood, China) with a 785 nm laser.

Binding Free Energy Calculation. We used AutoDock Tools[37] to calculate the free energy of molecular binding to RBD in simulation snapshots. RBD was used as a
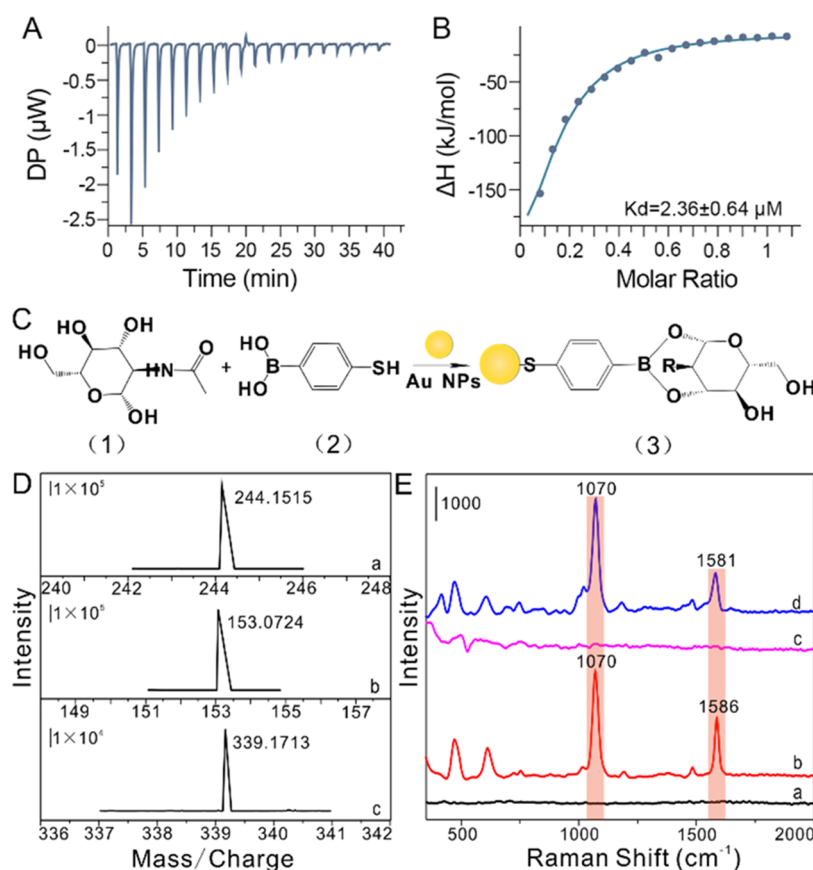
Figure 2. Surface material analysis of N-M-Au. (A, B) Results of the interaction between NAG and RBD were detected by ITC. (C) Reaction linker of NAG with MPBA and modification of AuNPs: (1) NAG, (2) MPBA, and (3) NAG-MPBA-AuNPs (R = −HCOCH$_3$). (D) Mass spectrometry results of NAG, MPBA, and NAG-MPBA. (a) ESI-MS spectrum of NAG (M + Na$^+$): m/z = 244, (b) ESI-MS spectrum of MPBA (M−H$^+$): m/z = 154, and (c) ESI-MS spectrum of NAG-MPBA (M): m/z = 339 (detailed mass spectrometry data can be seen in Figure S7). (E) SERS signals of NAG, MPBA, and NAG-MPBA. (a) SERS signals of Au NP substrates, (b) MPBA, (c) NAG, and (d) their reaction products NAG-MPBA.

conformation-invariant receptor and the molecule as a conformation-changing ligand for semiflexible docking.

Isothermal Titration Calorimetry (ITC) Assay. ITC assays were carried out on a MicroCal VP-ITC calorimeter (Malvern) at 25 °C in PBS buffer with a pH of 7.4. The protein concentrations in the syringe and the cell were approximately 200 and 20 μM, respectively. Titration data were analyzed using the Origin 8.0 program and fitted by a one-site binding model.

Analytical Application of the Fishing Mode Device to RBD in Human Blood. Standard add-on RBD analysis was performed on human blood samples from five healthy individuals. The blood was centrifuged at 12000g for 5 min at 4 °C, and the supernatant was obtained RBD containing serum for subsequent detection. For comparison, serum samples were measured with a commercial enzyme-linked immunosorbent assay (ELISA) kit with a microplate reader (Sino Biological Inc. China, KIT40592), and the procedure completely followed the protocol suggested for the commercial kit.

■ RESULTS AND DISCUSSION

Preparation of AgAN-Au NP-Aptamer (AgAN-Au-Apt) in a Fishing Mode Device. We attempted to develop a fishing mode device for the detection of SARS-CoV-2 RBD and combine the characteristics of RBD to precisely control

the SERS hotspots and achieve specific, sensitive, and stable detection of RBD. The first step is to attach AuNPs to AgAN and modify aptamers on AuNPs (Figure 1A). Previous studies have found that AuNPs modified on acupuncture needles can be used for ultrasensitive and highly repetitive SERS detection,[33] and dopamine was detected in complex samples.[32] Therefore, we adopted an acupuncture needle as our detection platform because it is portable and easy to sample. While there are two types of commonly used acupuncture needles, steel and Ag needles, we conducted a trial on each type separately to identify the best application platform. Both acupuncture needles were immersed in a concentrated solution of PVP-AuNPs with a uniform particle size of 55 nm (Figure S1). The surface of the acupuncture needle was rough, and AuNPs were easily, densely, and firmly attached to the acupuncture needle.[32] Figure S2 shows AuNPs modified on steel and Ag needles, respectively, and it can be seen that the attachment efficacies of AuNPs on the two needles are essentially the same, but examination with CV (1 × 10^{-6} M) revealed that SERS enhancement for AuNPs attached to the Ag acupuncture needle (AgAN) was 4−5 times stronger than that for AuNPs adsorbed on common steel needles (Figure S3). We believe that this is due to the formation of a double-coupled electromagnetic field between the silver layer and the AuNPs.[38] Therefore, we chose to use AgAN as the detection platform of our fishing mode device. Figure 1B,C shows that
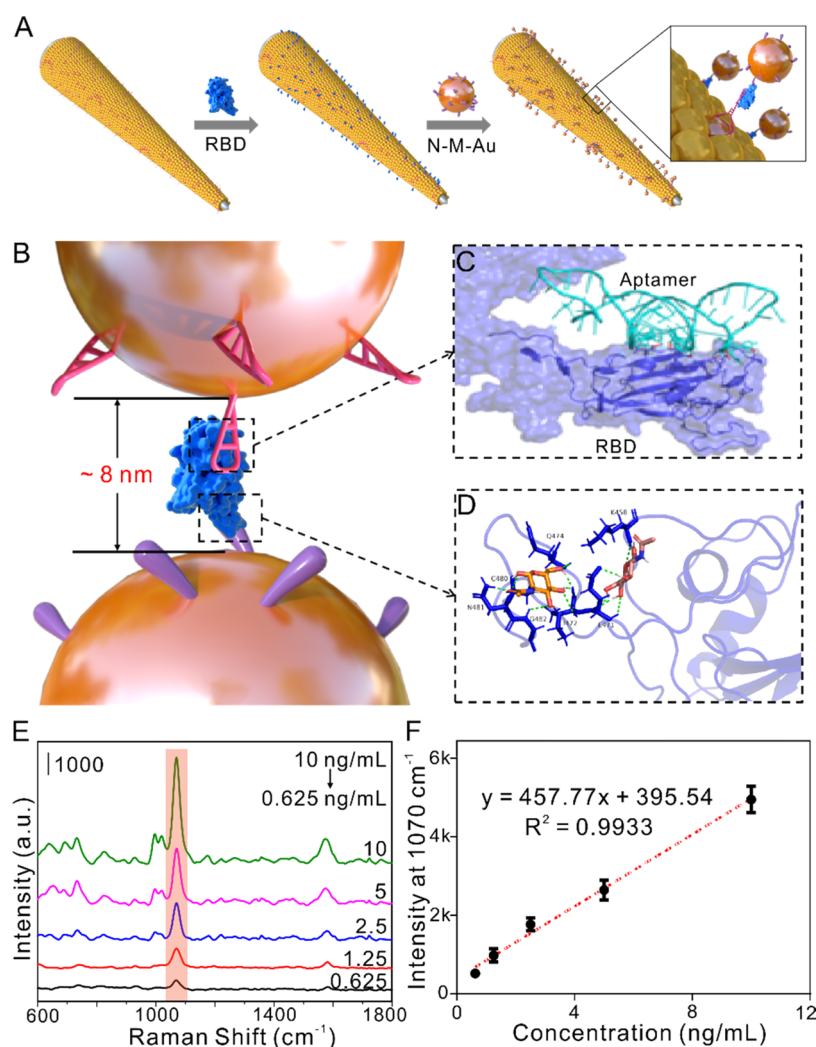
Figure 3. Detection principle and results of RBD are introduced. (A) Fishing model device formation. The AgAN-Au-Apt was connected with RBD, and N-M-Au was added to form a complete fishing mode device (AgAN-Au-Apt-RBD-N-M-Au). (B) Structure diagram of AgAN-Au-Apt-RBD-N-M-Au with a gap of about 8 nm after assembly. (C) Schematic diagram of binding of the aptamer to RBD.[22] (D) Schematic of the two binding sites of NAG to the RBD. (E) SERS detection signals of the fishing mode device for different concentrations of RBD were 0.625, 1.25, 2.5, 5, and 10 ng/mL. (F) SERS peak intensities at 1070 cm^{-1} versus RBD concentrations according to the spectra shown in (E). Error bars represent ± SD (n = 3).

AuNPs were densely attached to the surface of AgAN and assembled into AgAN-Au. SERS-enhanced response and stability detection were carried out with CV (1×10^{-6} M), as shown in Figure 1D,E. It can be concluded that the prepared AgAN-Au has a strong SERS effect and high stability.

The application of molecular aptamers for nucleic acid recognition has many advantages for the study and detection of SARS-CoV-2.[39,40] The smaller aptamer allows for less steric hindrance on the surface of the coronavirus. In theory, the smaller size allows for the binding of more recognition molecules on the same surface area of coronavirus,[41] so the use of aptamers for RBD-specific capture was chosen in our designed fishing mode device. The SARS-CoV-2 RBD is the protein thought to recognize and bind to different host receptors.[42] The purified protein was sequenced and compared with the RBD sequence in the NCBI database, which was consistent with the RBD sequence in the NCBI database (Figure S4). It was verified that the RBD used in this experiment was SARS-CoV-2 RBD. Song et al.[22] reported several aptamers that specifically bind to the SARS-CoV-2

RBD, and we selected one of the most strongly binding aptamers, CoV-2-RBD-1C (the dissociation constant (K_d) of the CoV-2-RBD-1C aptamer was 5.8 ± 0.8 nM). We examined the binding interaction and affinity of the aptamer for the RBD by ITC (Figure 1F,G), which revealed a K_d of 10.1 ± 3.35 nM. This result showed that the aptamer has a strong affinity for the RBD, and it is largely consistent with literature reports.[22] It also verified that the binding of the aptamer to the RBD was in accordance with our design idea, and the high affinity allowed specific detection of the RBD protein in subsequent work. It is known that amino (−NH$_2$) groups have a high affinity for Au.[43] In the synthesis of the aptamer, the amino group was modified on its 5′ end, and the aptamer was supported on AuNPs with surface amino groups to form Au-Apt. To verify whether the aptamers were modified on the AuNPs, we attached the synthesized aptamers with Cy3 fluorescent molecules; after the aptamers reacted with AuNPs, a fluorescence microscope was used before and after the reaction to determine whether the AuNPs exhibited fluorescence. As shown in Figure S5, the AuNPs modified with the fluorescent

aptamer and washed sufficiently still exhibited fluorescence, while the AuNPs without modification of the aptamer were nonfluorescent. In addition, in Figure 1H,I, compared with the unmodified aptamer (Figure 1B), Figure 1H becomes blurred. Because the aptamer belongs to organic molecules with poor conductivity, it will be blurred in the SEM micrograph, which further proves that the aptamer is modified on AuNPs. Therefore, we modified the aptamer with AgAN-Au to form AgAN-Au-Apt. This provided the first work for detecting RBD in the next step.

Preparation of NAG-MPBA-AuNPs (N-M-Au) in a Fishing Mode Device. We obtained molecular interaction data between NAG and RBD from the RCSB-PDB database (ID: 6ym0). Analysis of RBD binding to NAG with AutoDock Tools[37] indicated that NAG and RBD have a binding role (Figure S6). Two binding sites between NAG and RBD were found by simulation calculations, and their binding free energies are (1) −6.51 kcal/mol and (2) −6.44 kcal/mol, respectively. The equilibrium dissociation constants (K_d) of the two binding sites were calculated to be on the order of micromolar: (1) 17.04 μM and (2) 19.02 μM (Figure S6). The ITC test showed (Figure 2A,B) that NAG and RBD establish a binding force ($K_d = 2.36 \pm 0.64$ μM), which also indicates that NAG binding to the RBD is in accordance with the computational results and produces a linkage. The design theory of the present work is also supported by experimental data indicating that NAG has an affinity response to RBD. NAG was linked with MPBA as in previous studies,[34−36] and the conjugates were supported on the periphery of AuNPs (N-M-Au) (Figure 2C). As shown by mass spectrometry data in Figures 2D and S7, NAG reacted with MPBA to produce NAG-MPBA. NAG-MPBA plays a connecting role with the AuNPs and acts as a beacon molecule. Raman signals and SERS signals of NAG and MPBA as well as the postreaction linkage were detected. NAG had no significant Raman and SERS signals. The SERS signal of MPBA was observed to have two characteristic peaks at 1070 and 1586 cm^{-1}, which were derived from a breathing mode combined with C−S stretching and C-ring stretching and a mode coupling B−C stretching and C-ring stretching, respectively,[44] and the same was true for the SERS signals of NAG-MPBA (Figure 2E). After dehydration and condensation of NAG with MPBA, the peak for NAG-MPBA at 1586 cm^{-1} was red-shifted to 1581 cm^{-1}. We used the SERS signal at 1070 cm^{-1} as the main signal marker. From the results in Figure S8, it can be seen that different concentrations of NAG-MPBA-modified AuNPs and their signal intensities changed accordingly. As the concentration of NAG-MPBA increased, the final output signal became stronger, and after the concentration of NAG-MPBA exceeded 1×10^{-5} M, AuNPs agglomerated and could not be used in the fishing mode device. Therefore, we supported NAG-MPBA (1×10^{-5} M) on AuNPs through thiol modification on MPBA to form N-M-Au. The characterization of N-M-Au showed (Figure S9) that N and S elements were observed in the energy spectrum of AuNPs modified by NAG-MPBA, while the spectrum of PVP-AuNPs did not show the appearance of N and S elements. We believe that N-M-Au preparation was completed.

Formation of the Fishing Mode Device for RBD Detection. The more labile signal output of SERS when it is induced in the vicinity of biological molecules makes detection difficult, and the limit of detection cannot be lowered, which may be caused by the formation of random and heterogeneous hotspots.[45] Therefore, fishing mode devices with high sensitivity, specificity, and reproducibility need to construct stable hotspots to ensure a stable output of the signal in addition to low concentrations and specific recognition in the test. Based on this, we attempted to build accurate SERS hotspots for the fishing mode device used to detect the SARS-CoV-2 RBD (Figure 3A). Our fishing mode device consists of two parts: (1) AgAN-Au-Apt that can fish RBD; (2) AgAN-Au-Apt-RBD that can further fish N-M-Au. We determined the spatial resolution of the RBD as 4−6 nm with data from the RCSB-PDB database (ID: 6YM0, Figure S10A). Using binding modes provided in previous reports, we simulated the binding of the aptamer with the RBD and found that the spatial structure was relatively precise after binding (Figure S10B), which is beneficial for the formation of hotspots between AuNPs at the rear. Therefore, the complete fishing mode device captures and immobilizes the RBD through AgAN-Au-Apt and forms a solid structure with AuNPs on the AgAN through the combination of N-M-Au and RBD. The distances between AuNPs are in the range 6−9 nm (∼8 nm, i.e., the aptamer diameter is approximately 2−3 nm, and the average RBD diameter is 5 nm, approximately 8 nm after assembling together), which constructs stable SERS hotspots. We mixed Au NP-aptamer (Au-Apt), RBD, and N-M-Au in a PBS solution. Because of their interactions, the NPs connected with each other. As shown in Figure S11, after two kinds of AuNPs were connected by the RBD, we found by SEM that the distance between the two AuNPs (Au-Apt-RBD-N-M-Au) was maintained within 10 nm (the average wavelength is about 8 nm), which verified the assembly of SERS hotspots. As shown in Figure 3B, two kinds of AuNPs are connected with the aptamer and NAG-MPBA through RBD, forming a gap of about 8 nm, which perfectly forms the SERS hotspots and can complete the detection of RBD. If there is no RBD, the hotspots cannot be formed, and there is no corresponding SERS signal. It can be seen from Figure 3C that the aptamer binds to RBD in its spatial binding state. Figure 3D also shows the binding site of NAG and RBD. The assembly principle of the fishing mode device is further revealed. Also, Figure S12 shows the electromagnetic enhancement when the gap between AuNPs is ∼8 nm, and the hotspots formed by the fishing mode device can output high-intensity and stable SERS signal. When we fished the RBD with AgAN-Au-Apt, we only needed to add N-M-Au to collect signals from beacons on N-M-Au. A significant beacon signal indicates that there is an RBD in the detection environment. This fishing mode device not only detects the SARS-CoV-2 RBD but also regulates SERS protein detection in biological neighborhoods to achieve optimal detection. The control of spacing between NPs to less than 10 nm has been highly pursued for SERS detection,[1,4] and the present fishing mode device is in a position to achieve precise control of NP spacing by utilizing the properties of the RBD protein and its spatial size to complete construction of stable SERS hotspots for use in detection of the RBD.

Operation of the fishing mode device was divided into two steps. In the first step, RBD (2.5 ng/mL) was added to a PBS solution (pH = 7.4), and AgAN-Au-Apt was placed in a solution environment containing RBD for 10 min at 37 °C. AuNPs of the aptamer were modified on AgAN to fish RBD specifically and form AgAN-Au-Apt-RBD. Then, the AgAN-Au-Apt-RBD was cleaned with PBS three times to remove nonspecific adsorption material. In the second step, AgAN-Au-Apt-RBD was placed in a solution containing N-M-Au, and N-
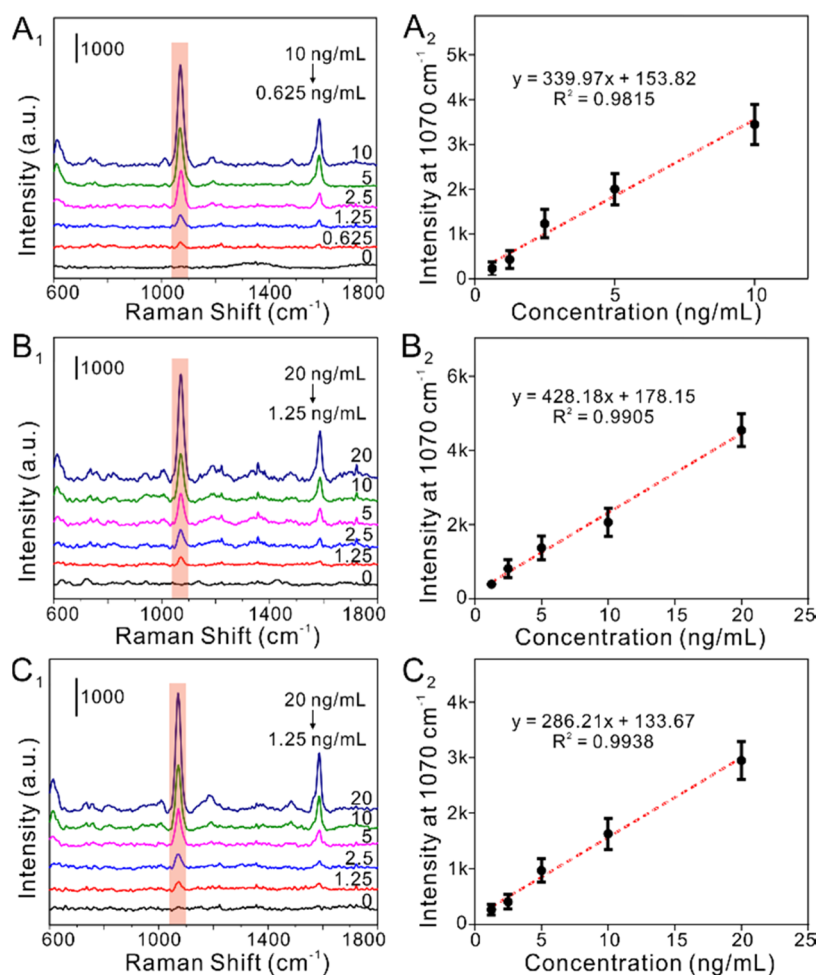
Figure 4. Fishing mode device detects RBD in different environments. (A1) RBD standard is added to polyproteins (extracted from HCT116 cells) + PBS environments, and the SERS signal collected by detecting the RBD under each concentration using the fishing mode device. (A2) Intensity of SERS peak at 1070 cm^{-1} versus RBD concentration was statistically determined from the spectra shown in (A1) (RBD with concentrations ranging from 0.625 to 10 ng/mL). (B1) SERS signals of different concentrations of the RBD standard added to the urine environment by the fishing mode device. (B2) Intensity of the SERS peak at 1070 cm^{-1} versus RBD concentration was statistically determined from the spectra shown in (B1) (RBD with concentrations ranging from 1.25 to 20 ng/mL). (C1) SERS signals of different concentrations of RBD standard added to the blood environment by fishing mode device. (C2) Intensity of SERS peak at 1070 cm^{-1} versus RBD concentration was statistically determined from the spectra shown in (C1) (RBD with concentrations ranging from 1.25 to 20 ng/mL).

M-Au was adsorbed on AgAN-Au-Apt-RBD through the binding of NAG and RBD. The complete fishing mode device was added to the RBD in PBS, and detection resulted in a significant SERS signal. Upon mixing the device in PBS solution with different concentrations of RBD, the signal strength exhibited a linear relationship. By exploring the detection limit of the fishing mode device, we determined that the SERS signal was still detected with an RBD concentration of 0.625 ng/mL (Figure 3E). Detection of different concentrations of RBD through SERS signal statistics shows that the fishing mode device is sensitive for the detection of RBD (Figure 3F). To probe reproducibility, five batches of fishing mode devices were prepared, and three fishing mode devices were removed from each batch to detect RBD (2.5 ng/mL) added to a PBS solution. Figure S13 shows that the detection results for each batch were similar, and the fishing mode device exhibited high reproducibility in RBD detection. We then explored whether the fishing mode device exhibited specificity in the detection of the RBD and tested the intact RBD and the denatured RBD. The results showed that the fishing mode device only provided a SERS signal for the intact

RBD (Figure S14). The detection unit of this fishing mode device has two important binding reactions. We replaced the specific aptamer and did not use NAG for detection. The results showed that only in the presence of the specific aptamer and the complete fishing mode device element was there a significant SERS signal, indicating that the fishing mode device exhibited specific detection of the RBD protein (Figure S15).

Fishing Mode Device for RBD in a Complex Environment. Detection of RBDs in different complex environments is the best way to examine the functioning of the present fishing mode device. We therefore mixed the RBD into different detection environments to explore its sensitivity and environmental adaptability. After first mixing different concentrations of the RBD with bovine serum albumin (BSA) solution (1 mg/mL, PBS solution), as shown in Figure S16, the present fishing mode device accomplished RBD detection at 0.625 ng/mL, and the detection signal strength exhibited a linear relationship with concentration. Next, by mixing different concentrations of the RBD with polyproteins extracted from the colon cancer cell line HCT116, we still observed detection of the RBD at 0.625 ng/mL (Figure 4A).

Finally, we mixed different concentrations of the RBD in urine and blood, and the results showed that the present fishing mode device achieved detection of the RBD with concentrations as low as 1.25 ng/mL in complex body fluid environments containing urine and blood, and RBD detection in both environments exhibited linear relationships (Figure 4B,C). The detection results show that in an environment without added RBD, there is no significant SERS signal, while in the presence of the RBD in different environments, the fishing mode device generates a significant SERS signal. In a relatively simple solution environment (protein-containing PBS solution), detection of the RBD by the fishing mode device is more effective than it is in the complex environment, which has a lower detection limit. We believe that the complex environment affects the binding of the aptamer to the RBD, possibly because other components in the environment cause steric hindrance of both in the binding region, reduce the number of RBD bonds to the aptamer, and lead to a decrease in the amount of N-M-Au adsorbed, thus reducing the signal intensity. However, the fishing mode device still exhibits relatively sensitive detection and is suitable for different detection environments. To establish whether the detection elements in the fishing mode device would provide false positives in detection, each element in the fishing mode device was paired to carry out SERS detection, and the results showed that a significant SERS signal appeared only with the complete fishing mode device; without any single unit, the fishing mode device exhibited no detection of the RBD (Figure S17). When used in a biofluid environment, the presence of a large number of other proteins will sterically hinder the binding of the aptamer in the fishing mode device to the RBD. However, the results showed that although there was some signal reduction, the detection of the RBD in complex environments still showed specificity and sensitivity. Because the fishing mode device was designed for specific capture of the RBD, detection was achieved by fishing with N-M-Au to form hotspots.

Operation of the fishing mode device was divided into two steps: the sampler adsorbed RBD in PBS with standard addition of RBD (2.5 ng/mL) and N-M-Au was connected. The overall detection time was the sum of the times for these two steps. By controlling different detection times, the results showed that the fishing mode device detected the RBD within 15 min (Figure S18). Compared with the involvement of professional laboratories and staff, the device is portable, inexpensive, rapid, and easy to operate, which is more in line with the need for on-site detection. ELISA is a traditional and commonly used protein detection method.[46] By comparing the fishing mode device with ELISA for RBD detection, detection by this fishing mode device can be verified. When using this fishing mode device and a commercial RBD ELISA kit to detect 2 ng/mL RBD in the blood of 5 healthy volunteers at the same time, the two detection effects were similar (Table S1). Of course, the time efficiency of the fishing mode device is also an important index of its detection ability. It is well known that the minimum ELISA detection time of 4−6 h is quite substantial, so our device was tested to establish the detection time (15 min). Based on the specificity and sensitivity of AgAN-Au-Apt for RBD fishing, N-M-Au was further fished, and stable hotspots (AgAN-Au-Apt-RBD-N-M-Au) were formed to achieve rapid detection of RBD in the environment.

CONCLUSIONS

In summary, we developed a highly sensitive and specific fishing mode device for the detection of the SARS-CoV-2 RBD in different environments. We found new SERS detection methods that exploit protein properties and spatial sizes to design hotspots that are architecturally stable for the detection of proteins. The use of an aptamer that specifically recognizes and captures the SARS-CoV-2 RBD together with a small compound (NAG) that binds to the RBD allowed the two to function as a fishhook to bring the two AuNPs into close connection and form hotspots with a gap of approximately 8 nm and produce a stable RBD detection signal. This method is not only simple and sensitive but can also achieve rapid (15 min) and low concentration (0.625 ng/mL) detection of RBD. At the same time, 0.625 ng/mL RBD could be detected in the mixed protein solution, and 1.25 ng/mL RBD could be detected in urine and blood environment. After a simple sampling and reaction process, the detection work can be completed in the portable Raman spectrometer, which can meet the field detection work in a variety of scenarios. Our work highlights the theoretical idea of the hotspots of precise control pursued in SERS detection and believes that the design and working concept of the present method open up a promising future for the application of SERS in a wide range of fields.

ASSOCIATED CONTENT

Ⓢ Supporting Information

The Supporting Information is available free of charge at https://pubs.acs.org/doi/10.1021/acs.analchem.1c03807.

> Further experimental details, characterization of AuNPs, characterization of AuNPs modified on steel and Ag needles, effect of AuNPs modified on steel and Ag needles on CV detection, alignment results of RBD protein sequences in the database, connection between fluorescent aptamers and AuNPs, recognition and interaction of small molecules NAG and RBD, mass spectrometry results of reaction products, SERS signal of AuNPs modified by different concentrations of MPBA-NAG, characterization of modified NAG-MPBA on AuNPs, RBD size and aptamer protein binding model, gap characterization of two kinds of AuNPs (Au-Apt-N-M-Au) connected with RBD, simulation of electromagnetic enhancement between two AuNPs with a gap of 8 nm, detection of RBD by different batch kits, specific detection before and after protein denaturation, specificity check of the fishing mode device, results were examined for RBD + BSA mixed solution, single unit of the fishing mode device and the SERS signal assembled with each other, time efficiency of detection kit for RBD detection, and comparison of the detection limits and detection times of different types of SARS-CoV-2 antigen detection methods (including Figures S1−S18 and Table S1) (PDF)

AUTHOR INFORMATION

Corresponding Authors

Pan Li − *Institute of Health and Medicine Technology, and Hefei Institutes of Physical Science, Chinese Academy of Sciences, Hefei 230031, China*; Email: lipan2011@iim.ac.cn

Hongzhi Wang − *Institute of Health and Medicine Technology, and Hefei Institutes of Physical Science, Chinese*

Academy of Sciences, Hefei 230031, China; University of Science and Technology of China, Hefei 230026, China; Cancer Hospital, Chinese Academy of Sciences, Hefei 230031, China; Email: wanghz@hfcas.ac.cn

Liangbao Yang − Institute of Health and Medicine Technology, and Hefei Institutes of Physical Science, Chinese Academy of Sciences, Hefei 230031, China; University of Science and Technology of China, Hefei 230026, China; Cancer Hospital, Chinese Academy of Sciences, Hefei 230031, China; ⓞ orcid.org/0000-0002-6559-6947; Email: lbyang@iim.ac.cn

Authors

Guangyao Huang − Institute of Health and Medicine Technology, and Hefei Institutes of Physical Science, Chinese Academy of Sciences, Hefei 230031, China; University of Science and Technology of China, Hefei 230026, China; Cancer Hospital, Chinese Academy of Sciences, Hefei 230031, China

Hongxin Zhao − High Magnetic Field Science Center, Hefei Institutes of Physical Science, Chinese Academy of Sciences, Hefei 230031, China

Juanjuan Liu − High Magnetic Field Science Center, Hefei Institutes of Physical Science, Chinese Academy of Sciences, Hefei 230031, China

Siyu Chen − Institute of Health and Medicine Technology, and Hefei Institutes of Physical Science, Chinese Academy of Sciences, Hefei 230031, China; University of Science and Technology of China, Hefei 230026, China

Meihong Ge − Institute of Health and Medicine Technology, and Hefei Institutes of Physical Science, Chinese Academy of Sciences, Hefei 230031, China; University of Science and Technology of China, Hefei 230026, China

Miao Qin − Institute of Health and Medicine Technology, and Hefei Institutes of Physical Science, Chinese Academy of Sciences, Hefei 230031, China; University of Science and Technology of China, Hefei 230026, China

Guoliang Zhou − Institute of Health and Medicine Technology, and Hefei Institutes of Physical Science, Chinese Academy of Sciences, Hefei 230031, China; University of Science and Technology of China, Hefei 230026, China

Yongtao Wang − Institute of Health and Medicine Technology, and Hefei Institutes of Physical Science, Chinese Academy of Sciences, Hefei 230031, China; University of Science and Technology of China, Hefei 230026, China

Shaofei Li − Institute of Health and Medicine Technology, and Hefei Institutes of Physical Science, Chinese Academy of Sciences, Hefei 230031, China; University of Science and Technology of China, Hefei 230026, China

Yizhuang Cheng − Institute of Health and Medicine Technology, and Hefei Institutes of Physical Science, Chinese Academy of Sciences, Hefei 230031, China; University of Science and Technology of China, Hefei 230026, China

Qiang Huang − Multiscale Research Institute of Complex Systems, Fudan University, Shanghai 201203, China; ⓞ orcid.org/0000-0001-5238-1704

Junfeng Wang − High Magnetic Field Science Center, Hefei Institutes of Physical Science, Chinese Academy of Sciences, Hefei 230031, China; ⓞ orcid.org/0000-0002-9608-6851

Complete contact information is available at: https://pubs.acs.org/10.1021/acs.analchem.1c03807

Author Contributions

Notes

The authors declare no competing financial interest.

■ ACKNOWLEDGMENTS

■ REFERENCES

(1) Li, J. F.; Huang, Y. F.; Ding, Y.; Yang, Z. L.; Li, S. B.; Zhou, X. S.; Fan, F. R.; Zhang, W.; Zhou, Z. Y.; Ren, B.; et al. Nature 2010, 464, 392−395.

(2) Alvarez-Puebla, R. A.; Liz-Marzan, L. M. Chem. Soc. Rev. 2012, 41, 43−51.

(3) Pérez-Jiménez, A. I.; Lyu, D.; Lu, Z.; Liu, G.; Ren, B. Chem. Sci. 2020, 11, 4563−4577.

(4) Camden, J. P.; Dieringer, J. A.; Wang, Y.; Masiello, D. J.; Marks, L. D.; Schatz, G. C.; Van Duyne, R. P. J. Am. Chem. Soc. 2008, 130, 12616−12617.

(5) Han, X. X.; Zhao, B.; Ozaki, Y. Anal. Bioanal. Chem. 2009, 394, 1719−1727.

(6) Vendrell, M.; Maiti, K. K.; Dhaliwal, K.; Chang, Y.-T. Trends Biotechnol. 2013, 31, 249−257.

(7) Xu, H.; Aizpurua, J.; Käll, M.; Apell, P. Phys. Rev. E 2000, 62, 4318−4324.

(8) Zong, C.; Xu, M.; Xu, L.-J.; Wei, T.; Ma, X.; Zheng, X.-S.; Hu, R.; Ren, B. Chem. Rev. 2018, 118, 4946−4980.

(9) Kao, Y.-C.; Han, X.; Lee, Y. H.; Lee, H. K.; Phan-Quang, G. C.; Lay, C. L.; Sim, H. Y. F.; Phua, V. J. X.; Ng, L. S.; Ku, C. W.; et al. ACS Nano 2020, 14, 2542−2552.

(10) Lim, W. Y.; Goh, C.-H.; Thevarajah, T. M.; Goh, B. T.; Khor, S. M. Biosens. Bioelectron. 2020, 147, No. 111792.

(11) Chen, C.; Zou, Z.; Chen, L.; Ji, X.; He, Z. Nanotechnology 2016, 27, No. 435102.

(12) Xu, S.; Ouyang, W.; Xie, P.; Lin, Y.; Qiu, B.; Lin, Z.; Chen, G.; Guo, L. Anal. Chem. 2017, 89, 1617−1623.

(13) Zhang, X.; Dhawane, A. N.; Sweeney, J.; He, Y.; Vasireddi, M.; Iyer, S. S. Angew. Chem. 2015, 127, 6027−6030.

(14) Flesch, J.; Bettenhausen, M.; Kazmierczak, M.; Klesse, W. M.; Skibitzki, O.; Psathaki, O. E.; Kurre, R.; Capellini, G.; Guha, S.; Schroeder, T.; et al. ACS Appl. Mater. Interfaces 2021, 13, 8049−8059.

(15) Sun, Y.; Xu, L.; Zhang, F.; Song, Z.; Hu, Y.; Ji, Y.; Shen, J.; Li, B.; Lu, H.; Yang, H. *Biosens. Bioelectron.* **2017**, *89*, 906−912.

(16) Wu, Y.; Choi, N.; Chen, H.; Dang, H.; Chen, L.; Choo, J. *Anal. Chem.* **2020**, *92*, 2628−2634.

(17) Lane, L. A.; Qian, X.; Nie, S. *Chem. Rev.* **2015**, *115*, 10489−10529.

(18) Zheng, Y.; Soeriyadi, A. H.; Rosa, L.; Ng, S. H.; Bach, U.; Gooding, J. J. *Nat. Commun.* **2015**, *6*, No. 8797.

(19) Choi, H.-K.; Park, W.-H.; Park, C.-G.; Shin, H.-H.; Lee, K. S.; Kim, Z. H. *J. Am. Chem. Soc.* **2016**, *138*, 4673−4684.

(20) Ryu, H.-J.; Lee, W. K.; Kim, Y. H.; Lee, J.-S. *Microchim. Acta* **2021**, *188*, No. 164.

(21) Guerrini, L.; Arenal, R.; Mannini, B.; Chiti, F.; Pini, R.; Matteini, P.; Alvarez-Puebla, R. A. *ACS Appl. Mater. Interfaces* **2015**, *7*, 9420−9428.

(22) Song, Y.; Song, J.; Wei, X.; Huang, M.; Sun, M.; Zhu, L.; Lin, B.; Shen, H.; Zhu, Z.; Yang, C. *Anal. Chem.* **2020**, *92*, 9895−9900.

(23) Xiang, S.; Ge, C.; Li, S.; Chen, L.; Wang, L.; Xu, Y. *ACS Appl. Mater. Interfaces* **2020**, *12*, 28985−28992.

(24) Liu, Y.; Tian, H.; Chen, X.; Liu, W.; Xia, K.; Huang, J.; de la Chapelle, M. L.; Huang, G.; Zhang, Y.; Fu, W. *Microchim. Acta* **2020**, *187*, No. 160.

(25) Li, Y.; Fang, Q.; Miao, X.; Zhang, X.; Zhao, Y.; Yan, J.; Zhang, Y.; Wu, R.; Nie, B.; Hirtz, M.; et al. *ACS Sens.* **2019**, *4*, 2605−2614.

(26) Amanat, F.; Stadlbauer, D.; Strohmeier, S.; Nguyen, T. H.; Chromikova, V.; McMahon, M.; Jiang, K.; Arunkumar, G. A.; Jurczyszak, D.; Polanco, J.; et al. *Nat. Med.* **2020**, *26*, 1033−1036.

(27) Hui, D. S.; Azhar, E. I.; Madani, T. A.; Ntoumi, F.; Kock, R.; Dar, O.; Ippolito, G.; Mchugh, T. D.; Memish, Z. A.; Drosten, C.; et al. *Int. J. Infect. Dis.* **2020**, *91*, 264−266.

(28) Wu, J. T.; Leung, K.; Leung, G. M. *Lancet* **2020**, *395*, 689−697.

(29) Martín, J.; Tena, N.; Asuero, A. G. *Microchem. J.* **2021**, *165*, No. 106305.

(30) Li, W.; Moore, M. J.; Vasilieva, N.; Sui, J.; Wong, S. K.; Berne, M. A.; Somasundaran, M.; Sullivan, J. L.; Luzuriaga, K.; Greenough, T. C.; et al. *Nature* **2003**, *426*, 450−454.

(31) Chen, Y.; Guo, Y.; Pan, Y.; Zhao, Z. J. *Biochem. Biophys. Res. Commun.* **2020**, *525*, 135−140.

(32) Li, P.; Zhou, B.; Cao, X.; Tang, X.; Yang, L.; Hu, L.; Liu, J. *Chem. - Eur. J.* **2017**, *23*, 14278−14285.

(33) Zhou, B.; Mao, M.; Cao, X.; Ge, M.; Tang, X.; Li, S.; Lin, D.; Yang, L.; Liu, J. *Anal. Chem.* **2018**, *90*, 3826−3832.

(34) Deshayes, S.; Cabral, H.; Ishii, T.; Miura, Y.; Kobayashi, S.; Yamashita, T.; Matsumoto, A.; Miyahara, Y.; Nishiyama, N.; Kataoka, K. *J. Am. Chem. Soc.* **2013**, *135*, 15501−15507.

(35) Kim, H.; Kang, Y. J.; Kang, S.; Kim, K. T. *J. Am. Chem. Soc.* **2012**, *134*, 4030−4033.

(36) Liu, H.; Li, Y.; Sun, K.; Fan, J.; Zhang, P.; Meng, J.; Wang, S.; Jiang, L. *J. Am. Chem. Soc.* **2013**, *135*, 7603−7609.

(37) Morris, G. M.; Huey, R.; Lindstrom, W.; Sanner, M. F.; Belew, R. K.; Goodsell, D. S.; Olson, A. J. *J. Comput. Chem.* **2009**, *30*, 2785−2791.

(38) Li, P.; Yan, X.; Zhou, F.; Tang, X.; Yang, L.; Liu, J. *J. Mater. Chem. C* **2017**, *5*, 3229−3237.

(39) Huang, M.; Yang, J.; Wang, T.; Song, J.; Xia, J.; Wu, L.; Wang, W.; Wu, Q.; Zhu, Z.; Song, Y.; et al. *Angew. Chem.* **2020**, *132*, 4830−4835.

(40) Teng, I.-T.; Li, X.; Yadikar, H. A.; Yang, Z.; Li, L.; Lyu, Y.; Pan, X.; Wang, K. K.; Tan, W. *J. Am. Chem. Soc.* **2018**, *140*, 14314−14323.

(41) Zhang, L.; Fang, X.; Liu, X.; Ou, H.; Zhang, H.; Wang, J.; Li, Q.; Cheng, H.; Zhang, W.; Luo, Z. *Chem. Commun.* **2020**, *56*, 10235−10238.

(42) Shang, J.; Ye, G.; Shi, K.; Wan, Y.; Luo, C.; Aihara, H.; Geng, Q.; Auerbach, A.; Li, F. *Nature* **2020**, *581*, 221−224.

(43) Mandal, T. K.; Fleming, M. S.; Walt, D. R. *Nano Lett.* **2002**, *2*, 3−7.

(44) Yang, D.; Afroosheh, S.; Lee, J. O.; Cho, H.; Kumar, S.; Siddique, R. H.; Narasimhan, V.; Yoon, Y.-Z.; Zayak, A. T.; Choo, H. *Anal. Chem.* **2018**, *90*, 14269−14278.

(45) Jiang, Z.; Jiang, X.; Su, S.; Wei, X.; Lee, S.; He, Y. *Appl. Phys. Lett.* **2012**, *100*, No. 203104.

(46) Wu, L.; Li, G.; Xu, X.; Zhu, L.; Huang, R.; Chen, X. *TrAC, Trends Anal. Chem.* **2019**, *113*, 140−156.